

RESEARCH ARTICLE

Rnf220 cooperates with Zc4h2 to specify spinal progenitor domains

Jumee Kim^{1,*}, Tae-Ik Choi^{2,*}, Shinye Park³, Myung Hee Kim³, Cheol-Hee Kim^{2,‡} and Seunghee Lee^{1,‡}

ABSTRACT

During early embryonic development of the spinal cord, graded sonic hedgehog signaling establishes distinct ventral progenitor domains by regulating the spatiotemporal expression of fate-specifying transcription factors. However, regulation of their protein stability remains incompletely understood. Here, we show that RNF220, an E3 ubiquitin ligase, plays crucial roles in the generation of the ventral progenitor domains, which produce ventral interneurons and motor neurons, by targeting key transcription factors including Dbx1/2 and Nkx2.2 for degradation. Surprisingly, RNF220 interacts with, and is co-expressed with, a zinc-finger protein ZC4H2, and they cooperate to degrade Dbx1/2 and Nkx2.2. RNF220-null mice show widespread alterations of ventral progenitor domains, including the loss of the p2 domain that produces V2 interneurons. Knockdown of RNF220 and ZC4H2 in the chick spinal cord downregulates expression of the V2 interneuronal marker Chx10. Co-expression of RNF220 and ZC4H2 further promotes the ability of Nkx6.1 to induce ectopic Chx10⁺ V2 interneurons. Our results uncover a novel regulatory pathway in establishing distinct progenitor domains through modulating the protein stability of transcription factors. Our results provide insights into the molecular mechanism by which ZC4H2 mutations lead to human syndromes characterized by delayed motor development.

KEY WORDS: Ventral spinal cord, RNF220, ZC4H2, p2 domain, V2 interneuron, Ubiquitylation, Mouse, Chick

INTRODUCTION

In the developing ventral spinal cord, progenitor cell populations in each specific progenitor domain give rise to a distinct type of neuron, which eventually contributes to motor circuits (Goulding and Lamar, 2000; Jessell, 2000). The identity of each ventral progenitor domain is determined by the combinatorial expression of homeodomain (HD) and basic-helix-loop-helix (bHLH) progenitor transcription factors in response to the gradient of sonic hedgehog (Shh) along the dorsal ventral axis (Briscoe et al., 2000; Ericson et al., 1995; Roelink et al., 1995). However, despite the advances in our understanding of the roles these transcription factors play in the patterning of progenitor domains, regulation of their protein

stability, and the contribution of this stability to progenitor cell type specification, remain incompletely understood.

As summarized in Fig. 1C, Dbx1⁺/Dbx2⁺/Nkx6.2⁻ progenitor domain (p) 0 progenitors generate Evx1/2⁺ V0 interneurons (V0 INs) (Pierani et al., 1999, 2001). Nkx6.2⁺/Dbx1⁻/Dbx2⁺ p1 progenitors generate En1⁺ V1 INs (Burrill et al., 1997; Vallstedt et al., 2001). Nkx6.1⁺/Irx3⁺/FoxN4⁺ p2 progenitors give rise to Chx10⁺ V2a- or Gata3⁺ V2b INs (Briscoe et al., 2000; Ericson et al., 1997b; Francius et al., 2015). Nkx2.2⁺/Nkx6.1⁺ p3 progenitors give rise to Sim1⁺ V3 INs (Borowska et al., 2013; Sun et al., 2003). The bHLH factor Olig2⁺ pMN progenitors generate motor neurons (MNs) and, later, oligodendrocytes (Lee et al., 2005; Ravanelli and Appel, 2015; Zhou and Anderson, 2002). Nkx6.1 is induced more broadly by Shh in the p3, pMN and p2 domains. Nkx6.1 plays a crucial role in the patterning and establishment of pMN and p2 domains, and therefore induces the generation of MN and V2 IN. Accordingly, ectopic expression of Nkx6.1 in the chick neural tube can trigger MN and V2 IN fates, whereas deletion of *Nkx6.1* in mice shows a complete failure in V2 IN generation, a marked reduction of MNs and the ectopic ventral expansion of Dbx2 in the regions where MNs and V2 INs are generated (Sander et al., 2000). The transcription factors expressed in the progenitor domains appear to further activate their downstream transcription factors that establish a transcriptional cascade to control various aspects of cell fate specification and development. For example, Lhx3 and Lhx4 are derepressed in the p2 domain. The LIM domains of Lhx3 interact with the nuclear LIM interacting factor (NLI, also known as Ldb and Clim). NLI has a self-dimerization domain, thereby leading to the formation of a tetrameric complex of 2NLI:2Lhx3, which in turn interacts with the promoters of genes that confer the V2a IN identity (Jurata et al., 1998; Thaler et al., 2002).

The E3 ubiquitin ligase RING-finger protein 220 (RNF220) has been demonstrated to target the transcriptional repressor Sin3B for ubiquitylation (Kong et al., 2010). RNF220 also promotes canonical Wnt signaling by stabilizing β -catenin through USP7-mediated deubiquitylation, suggesting its potential role in Wnt-related tumorigenesis (Ma et al., 2014). Although recent studies in cultured cells suggest that RNF220 mediates target substrate protein degradation or stabilization through ubiquitylation-dependent processes, it remains unexplored whether RNF220 functions as a key modulator of protein stability *in vivo*. Our results reveal not only a crucial role of RNF220 in patterning of spinal progenitor domains, but also a surprising interplay of RNF220 with ZC4H2. ZC4H2 is a zinc-finger protein that belongs to the family of proteins with a C-terminal zinc-finger domain characterized by four cysteine residues and two histidine residues. In mouse and zebrafish embryos, ZC4H2 is specifically expressed in the brain and spinal cord. Interestingly, expression of mutant forms of ZC4H2 reduces the number of dendritic spines in mouse primary hippocampal neurons, and knockdown of *zc4h2* in zebrafish results in impaired swimming, impaired MN development and a disorganized pattern

¹College of Pharmacy and Research Institute of Pharmaceutical Sciences, Seoul National University, Seoul 08826, Korea. ²Department of Biology, Chungnam National University, Daejeon 34134, Korea. ³Infection and Immunity Research Laboratory, Metabolic Regulation Research Center, Korea Research Institute of Bioscience and Biotechnology (KRIBB), Daejeon 34141, Korea.

*These authors contributed equally to this work

‡Authors for correspondence (zebrakim@cnu.ac.kr; leeseung@snu.ac.kr)

© C.-H.K., 0000-0002-3019-0699; S.L., 0000-0001-5483-0016

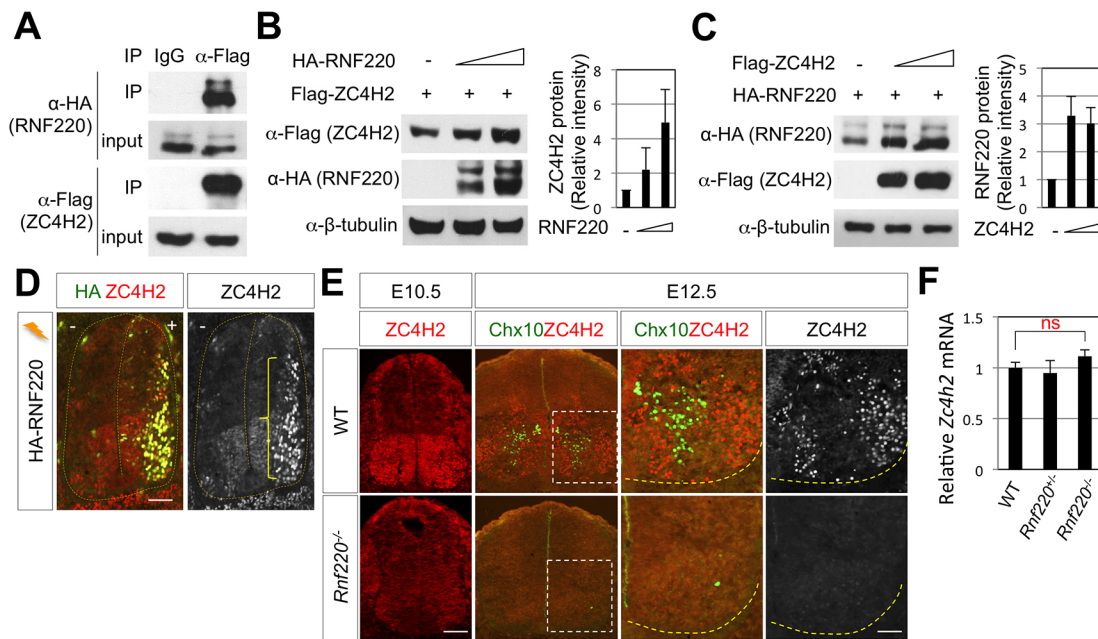


Fig. 2. RNF220 and ZC4H2 regulate each other's protein levels. (A) RNF220 interacts with ZC4H2. Co-immunoprecipitation assay with HEK293T cells transiently transfected with the expression vectors for HA-tagged RNF220 and Flag-tagged ZC4H2. (B) ZC4H2 is stabilized by RNF220. Stabilized ZC4H2 protein level quantified by western blotting of lysates of HEK293T cells transiently transfected with HA-RNF220 and Flag-ZC4H2. (C) RNF220 is stabilized by ZC4H2. Stabilized RNF220 protein level quantified by western blotting of lysates of HEK293T cells transiently transfected with HA-RNF220 and Flag-ZC4H2. (D) Ectopic induction of ZC4H2 expression (yellow bracket) in the lateral side of the spinal cord (thoracic level) following electroporation of HA-RNF220. +, electroporated side; -, non-electroporated side. (E) Loss of ZC4H2⁺ cells in the *Rnf220*^{-/-} spinal cord at E10.5 (thoracic level). Loss of Chx10⁺ cells and ZC4H2⁺ cells in the ventrolateral quadrant spinal cord (boxed area) in the *Rnf220*^{-/-} spinal cord (dashed lines) at E12.5 (thoracic level). IHC analyses with anti-ZC4H2 and anti-Chx10 antibodies. (F) qRT-PCR analysis of *Zc4h2* mRNA in the *Rnf220*^{-/-} spinal cord at E12.5. Data are presented as mean±s.d. of the relative mRNA levels of *Zc4h2* in WT, heterozygote and *Rnf220*^{-/-} spinal cord. ns, not significant. Scale bars: 100µm in D; 75µm in E E10.5 embryos; 50µm in E E12.5 embryos.

RNF220 protein levels were also enhanced by ZC4H2 (Fig. 2C). In the chick spinal cord, *in ovo* expression of RNF220 strongly induced ectopic expression of ZC4H2 in the lateral side of the spinal cord (Fig. 2D). We generated RNF220-null mice using the Clustered Regularly Interspaced Short Palindromic Repeats (CRISPR) and CRISPR-associated proteins (Cas) system with a single guide RNA (sgRNA) that targets exon7 of the *Rnf220* gene (Fig. 5A) (Jinek et al., 2012; Ran et al., 2013; Yang et al., 2014). Consistent with our chick results (Fig. 2D), the expression of ZC4H2 was almost eliminated in RNF220 deficient E10.5-E12.5 mouse spinal cords (Fig. 2E). Our qRT-PCR analyses revealed that the mRNA levels of *Zc4h2* were not altered in the *Rnf220*^{-/-} spinal cord relative to the wild-type (WT) spinal cord (Fig. 2F), suggesting that transcriptional regulation of *Zc4h2* is not modulated by RNF220. These results, together with the fact that RNF220 is an E3 ubiquitin ligase (Kong et al., 2010), suggest that RNF220 and ZC4H2 likely affect each other's protein stability.

Proteasomal degradation of ventral progenitor factors by RNF220

The interactions between ZC4H2 and RNF220 and their mutual control of protein stability raise an interesting possibility that RNF220 and ZC4H2 may cooperate to specify development of progenitor domains by targeting progenitor factors for degradation. Interestingly, we found that the protein levels of Dbx1, which is expressed in p0 cells, were reduced in the presence of RNF220 in a dose-dependent manner, and this reduction was further augmented by co-expressed ZC4H2 (Fig. 3A, quantification in right panel). We also obtained similar results for Dbx2 (data not shown) and other transcription factors such as Nkx2.2, Irx3, Nkx6.1 and FoxN4

(Fig. S2). Again, the protein levels of RNF220 were increased by ZC4H2 (Fig. 3A, compare lanes 2 and 3 with lanes 5 and 6). To further confirm whether Dbx2 is degraded by RNF220 and ZC4H2 through the proteasomal pathway, we used the proteasome inhibitor MG132, which blocked the degradation of Dbx2 (Fig. 3B). Next, to test whether Dbx2 and RNF220 interact with each other in cells, we performed coIP assays with HEK293T cell lysates transiently transfected with Myc-Dbx2 and HA-RNF220. HA-RNF220 was co-immunopurified with Myc-Dbx2 by anti-Myc antibody (Fig. 3C). We also found that Dbx1/2, Nkx2.2 and FoxN4 interact with RNF220, suggesting that Dbx1/2, Nkx2.2 and FoxN4 are likely new substrates of RNF220. Interestingly, Irx3 and Nkx6.1 did not interact with RNF220 and thus these factors may be regulated by RNF220 indirectly (data not shown).

We also tested whether ZC4H2 interacts with Dbx2 using *in vivo* GST-pull down assays. Interestingly, ZC4H2 interacted with Dbx2 only in the presence of RNF220 (Fig. 3D), suggesting that ZC4H2 does not bind to Dbx2 directly, but forms a ternary complex through binding to RNF220, which in turn recruits Dbx2. In HEK293T cells, we further found that Dbx2 was ubiquitylated, and that this ubiquitylation was enhanced by overexpressed RNF220 (Fig. 3E). Taken together, these results demonstrate that RNF220, together with ZC4H2, binds and ubiquitylates Dbx as a new substrate for degradation.

ZC4H2 is required for RNF220 to degrade Dbx2

To map the interaction interfaces between RNF220 and ZC4H2, we generated several deletion mutants and a W539R point mutant that lacks the ligase activity (Ma et al., 2014) (Fig. 4A). Using the coIP assays, we identified that ΔN and ΔNΔR constructs, which lack the

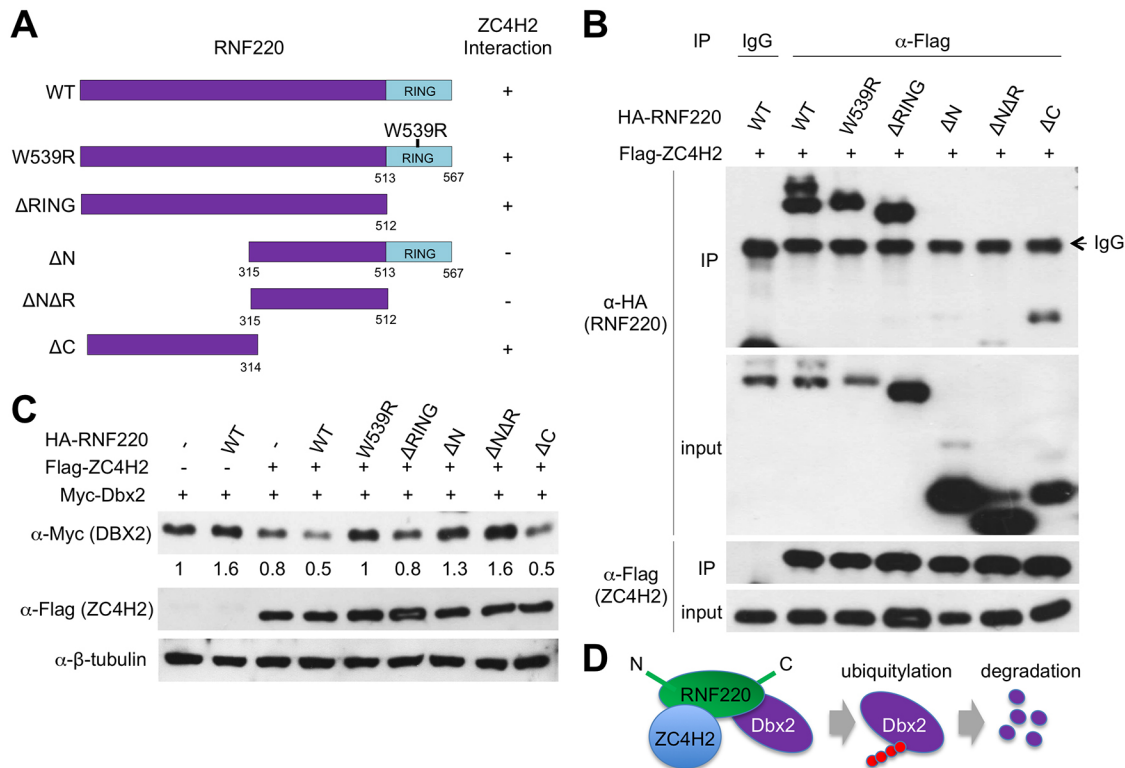


Fig. 4. Interaction between RNF220 and ZC4H2 is required to degrade Dbx2. (A) Schematic of the human RNF220 truncated constructs and W539R mutant. Right-hand side indicates the interaction of RNF220 with ZC4H2. -, no interaction; +, interaction. (B) Whereas RNF220 WT, W539R, Δ RING and Δ C interacted with ZC4H2, Δ N and Δ N Δ R of RNF220 showed no interaction with ZC4H2. (C) Degradation of Dbx2 by RNF220 WT, deletion constructs and W539R mutant in the presence of ZC4H2. The protein levels of Dbx2 were decreased to almost 50% (lanes 1 and 4). RNF220-W539R mutant lost the ability to degrade Dbx2 (lane 5). Dbx2 was not degraded by Δ N, whereas Dbx2 levels were increased by Δ N Δ R (lanes 7 and 8). Dbx2 was degraded by Δ RING and Δ C (lanes 6 and 9). The numbers indicate the relative levels of Dbx2 compared with the levels without RNF220 and ZC4H2. (D) Model for degradation of Dbx2 by RNF220 and ZC4H2. RNF220 and ZC4H2 mediate the ubiquitylation and proteasomal degradation of Dbx2.

time points (Figs 5B and 7A). First, to analyze whether RNF220 is required for the proliferation of the neural stem cells, we performed IHC with phosphohistone 3 (pH3) and BrdU labeling (Fig. 5B,C). Interestingly, compared with RNF220 WT and heterozygote embryos, *Rnf220*-null mutant embryos showed an increase of BrdU labeling and an expansion of Sox2⁺ progenitor cells in the ventral ventricular zone, in which V2 INs and MNs are generated, whereas the number of TuJ1⁺ (also known as Tubb3) neuronal cells in the ventro-lateral area was reduced (Fig. 5B,C), suggesting that RNF220 is likely to be involved in cell cycle exit and neuronal differentiation in ventral progenitor cells. We detected no significant cell death within the spinal cord of *Rnf220* mutants using IHC with cleaved caspase 3 antibody (Fig. 5C). We then examined the expression pattern of class I and II transcription factors in the spinal cord of *Rnf220*^{-/-} embryos. The Nkx2.2⁺ domain was expanded dorsally and the Nkx6.1⁺ domain was shifted ventrally, which resulted in a complete loss of the p2 progenitor domain and a narrower pMN domain marked by Olig2 expression at E9.5 (Figs 5B and 6A). We observed that the number of Nkx2.2⁺ cells was increased in *Rnf220*^{-/-} embryos but not in *Rnf220*^{+/-} embryos, suggesting that the level of RNF220 expression from one allele is sufficient to suppress the expansion of the Nkx2.2⁺ p3 domain (Fig. 5B). The lack of RNF220 expression led to the expansion of the Nkx6.2⁺, Dbx2⁺ and Dbx1⁺ domains compared with WT embryos (Fig. 6A,C). At E10.5, we also confirmed the loss of the p2 domain by FoxN4 ISH and Ascl1 IHC, which are well-identified p2 markers (Fig. 6B,C). We observed that Prdm12, a specific marker of

the p1 domain, was significantly reduced in *Rnf220*^{-/-} embryos (Fig. 6B,C). Thus, the loss of *Rnf220* deregulates the pattern of expression for a subset of homeobox genes in ventral progenitor cells. Given the widespread alterations of the progenitor domain patterning in *Rnf220* mutants, we tested whether certain signaling pathways involved in progenitor patterning in the spinal cord are deficient in *Rnf220* mutants. We examined the expression of Shh and Ptch1 for Shh signaling, Axin2 for Wnt signaling, and Msx1/2 for BMP signaling and found no dramatic change of their expression in the mutant embryos compared with WT embryos (Fig. 6D). These results indicate that RNF220 is mainly required to establish proper progenitor domains, including the p2, p1 and pMN domains, and functions to limit the boundaries of p0 and p3 progenitor domains within the ventral spinal cord (Fig. 10A).

Abnormal ventral neuronal differentiation in the absence of the *Rnf220* gene

We next analyzed the generation of interneuron subtypes in the ventral neural tube of *Rnf220*-null embryos. The progenitor domains that express RNF220 within the ventral neural tube of WT embryos include p1, p2, p3 and pMN, which give rise to V1, V2 and V3 INs and MNs, respectively (Briscoe and Ericson, 1999; Briscoe et al., 2000; Ericson et al., 1997a,b; Goulding and Lamar, 2000; Pierani et al., 1999; Qiu et al., 1998) (Fig. 1A-C). We examined whether the generation of any of these neuronal classes is impaired in *Rnf220* mutants, focusing first on the generation of V2 INs, given our observation that the p2 progenitor domain was completely abolished

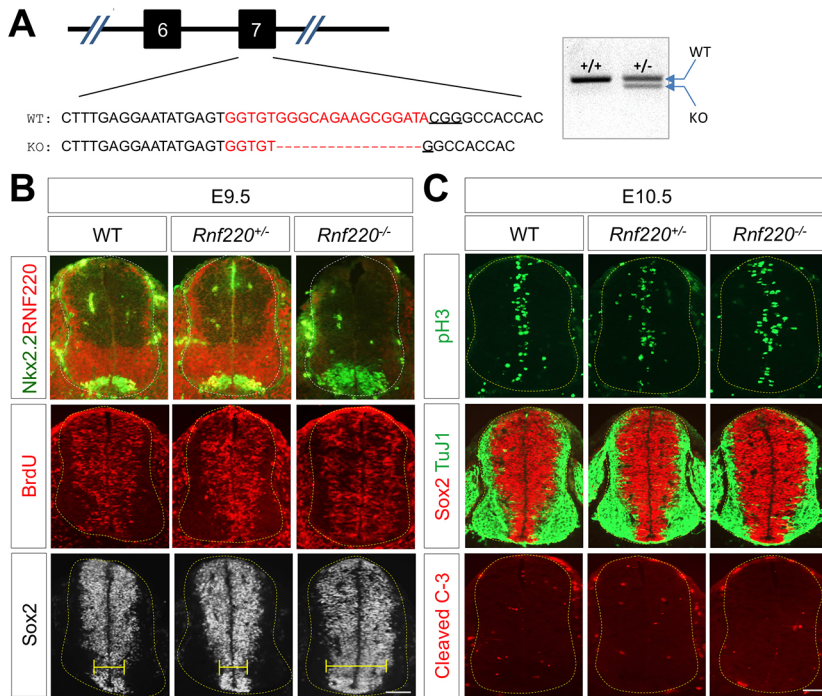


Fig. 5. *Rnf220*-null embryo shows increased *Sox2*⁺ progenitor cells but no change in apoptosis. (A) Schematic showing the CRISPR/Cas9-mediated *Rnf220* knockout mouse generation. Sequences for target exon7 of WT allele (upper) and *Rnf220* KO allele (lower). The target sequence of sgRNA is marked in red, and the PAM sequence is underlined. Genotyping PCR results show one DNA band for WT alleles from WT mouse genomic DNA and two DNA bands of WT and KO alleles from heterozygous mouse genomic DNA. (B,C) Immunohistochemistry with anti-RNF220, anti-Nkx2.2, anti-BrdU, anti-pH3, anti-*Sox2*, anti-TuJ1 and anti-cleaved caspase 3 (C-3) was performed on E9.5 and E10.5 mouse spinal cord (cervical level). Progenitor cells, marked by *Sox2*, are increased in the ventral ventricular zone (yellow bar), whereas neuronal cells, marked by TuJ1, are reduced in the ventrolateral area of spinal cord (dotted outline) in *Rnf220*^{-/-} mutant embryos compared with WT embryos. Scale bars: 50µm.

(Fig. 6B). At E12.5, *Rnf220* mutant embryos showed a dramatic reduction in the number of spinal V2 INs, as assessed by expression of the marker proteins *Chx10*, *Gata3*, *Sox14* and *Lhx3* (Al-Mosawie et al., 2007; Clovis et al., 2016; Del Barrio et al., 2007; Hargrave et al., 2000; Li et al., 2005; Muroyama et al., 2005) (Fig. 7A,D). The number of *Hb9*- (also known as *Mnx1*) expressing cells was also significantly reduced in *Rnf220* mutant embryos (Fig. 7A,D), which

correlates with the reduced pMN domain (Fig. 6A). Consistent with the reduction of *Prdm12* expression in the p1 progenitor domain, we found that *En1* expression was reduced in *Rnf220*^{-/-} mutant embryos when compared with WT embryos, using ISH with an *En1* antisense probe at E10.5 (Fig. 7B). Consistent with the expansion of *Nkx2.2*- and *Dbx1*-expressing progenitor domains, we detected a higher level of *Sim1* expression in V3 INs and an

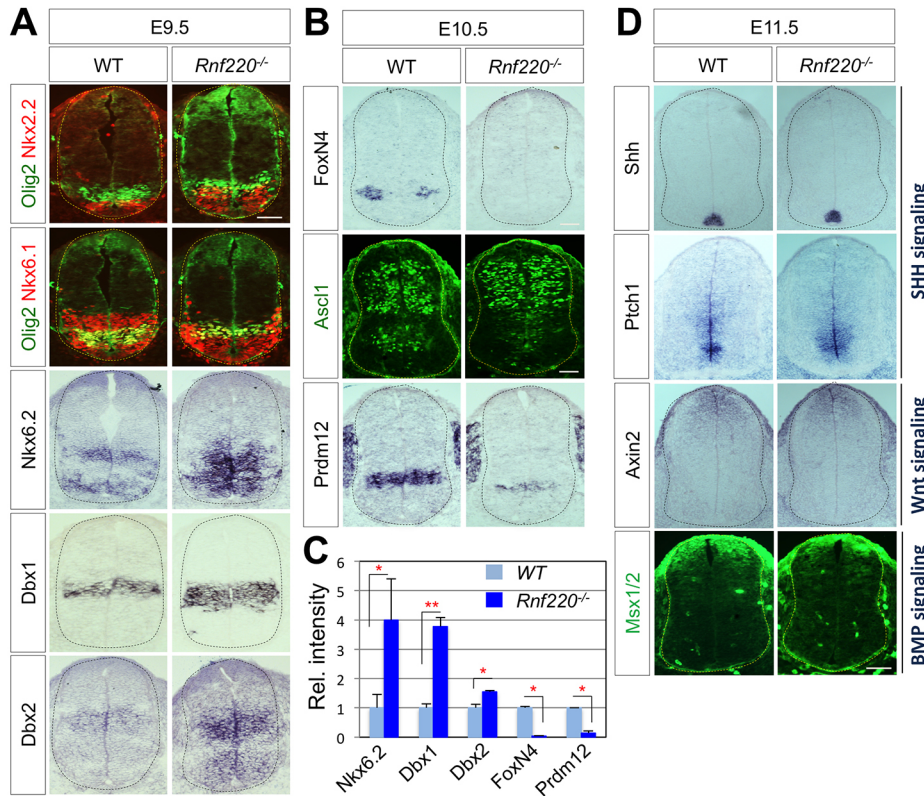


Fig. 6. RNF220 is crucial for proper progenitor domain formation. (A) The expression pattern of class I and II transcription factors in E9.5 *Rnf220*^{-/-} embryos (*n*=3) and their littermate controls (*n*=4) (cervical level). The *Nkx6.1*⁺ domain was shifted ventrally and the *Olig2*⁺ pMN domain was decreased, whereas the *Nkx2.2*⁺ p3 domain was expanded in *Rnf220*^{-/-} mutant embryos compared with WT embryos. *Nkx6.2*⁺, *Dbx1*⁺ and *Dbx2*⁺ domains were expanded in *Rnf220*^{-/-} mutant embryos compared with WT embryos. (B) ISH analyses of *FoxN4* and *Prdm12* and IHC with anti-*Ascl1* in E10.5 *Rnf220*^{-/-} embryos (*n*=4) and their littermate controls (*n*=5) (cervical level). The *FoxN4*⁺ and *Ascl1*⁺ p2 domain was lost and the *Prdm12*⁺ p1 domain was decreased in *Rnf220*^{-/-} mutant embryos. (C) Quantification was performed with multiple embryos as indicated and at least three sections from each embryo. Data are mean±s.d. **P*<0.05, ***P*<0.01 (Student's *t*-test). (D) ISH analyses of *Shh*, *Ptch1* and *Axin2* and IHC with anti-*Msx1/2* on E11.5 *Rnf220*^{-/-} embryos (*n*=4) and littermate controls (*n*=3) (cervical level). *Shh*, *Wnt* and *BMP* signaling was not affected in *Rnf220*^{-/-} mutant embryos. Dotted outlines indicate the border of the spinal cord. Scale bars: 50µm in A,B; 100µm in D.

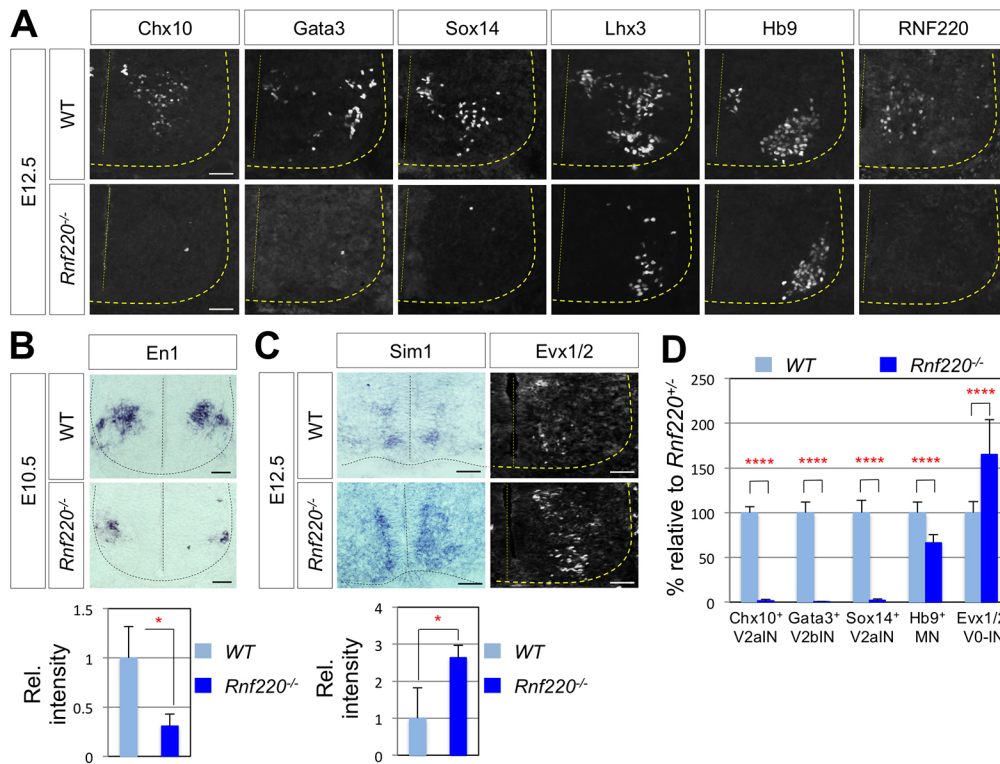


Fig. 7. Abnormal ventral neuronal differentiation in *Rnf220*-null embryonic spinal cord. (A) Chx10, Gata3, Sox14, Lhx3 and Hb9 expression in transverse sections at E12.5 in *Rnf220*-null embryos ($n=3$) and their littermate controls ($n=3$) (thoracic level). Ventrolateral quadrants of the spinal cord are shown in all panels. IHC with anti-RNF220 antibody confirms the absence of RNF220 expression in *Rnf220*-null embryos. (B) ISH analyses of *En1*⁺ V1 INs in E10.5 embryos (cervical level). (C) ISH analyses of *Sim1*⁺ V3 INs and immunostaining analyses of *Evx1/2*⁺ V0 INs in E12.5 embryos (thoracic level). Panels show the quantification of *En1*⁺ V1 INs in E10.5 and *Sim1*⁺ V3 INs in E12.5 embryos. Relative intensity of ISH signal was measured. Data are mean \pm s.d. * $P<0.05$ (Student's *t*-test). (D) Quantification of Chx10⁺ V2a INs, Gata3⁺ V2b INs, Sox14⁺ V2a INs, Hb9⁺ MNs and Evx1/2⁺ V0 INs in E12.5 embryos. Data are mean \pm s.d. **** $P<0.0001$ (Student's *t*-test). Scale bars: 50 μ m.

increased number of *Evx1/2*-expressing V0 INs in *Rnf220*^{-/-} mutant embryos, respectively (Fig. 7C,D). Notably, it is possible that neurons generated from altered progenitor domains of *Rnf220*^{-/-} mutant embryos may have additional defects, as we have examined only a limited number of markers.

RNF220 and ZC4H2 are required for proper generation of V2 INs

To further support the phenotypic results of *Rnf220* deletion in mouse embryos, we knocked down *Rnf220* and *Zc4h2* in developing chick embryos. We found reduced expression of ZC4H2, RNF220 and Nkx6.1 by knockdown constructs (Fig. S4). As expected, the number of Chx10⁺ V2a INs was dramatically reduced by knockdown of both *Rnf220* and *Zc4h2* genes in the developing chick neural tube (Fig. 8A,B). The number of Gata3⁺ V2b INs was also significantly affected by *Rnf220* and *Zc4h2* knockdown (Fig. 8A,B). In contrast, Hb9⁺ MNs were not significantly changed (Fig. 8A,B), and this may be because of low efficiency of the knockdown constructs. The complete loss of V2 INs in *Rnf220* mutant mouse embryos (Fig. 7A) and the reduction of V2 INs in chick knockdown embryos (Fig. 8A,B) suggest that RNF220 plays a role in establishing the p2 progenitor domain, affecting the subsequent V2 IN generation.

To test whether RNF220 alone is sufficient to support the development of p2 and V2 INs, we overexpressed HA-RNF220 in the chick neural tube. Interestingly, we found that there is <5% increase in Nkx6.1⁺ and Olig2⁺ progenitor cells and 2~3 ectopic Chx10⁺ and Hb9⁺ cells in the electroporated side compared with the control side (data not shown). These results indicate that RNF220 alone has minimal activity in determining the p2 domain. To identify other factors that RNF220 functions with to support the development of p2 and V2 INs, we analyzed Nkx6.1, which is required to establish progenitors for MN and V2 IN and to restrict the generation of V1 INs (Sander et al., 2000). When myc-Nkx6.1 alone was ectopically

overexpressed in one side of the chick neural tube, there was ~123% increase in the number of Chx10⁺ cells and ~117% increase in the number of Gata3⁺ cells compared with the unelectroporated control side (Fig. 9A,B). Co-expression of ZC4H2 did not facilitate the activity of Nkx6.1 in inducing Chx10 or Gata3 expression in the electroporated side compared with embryos that were electroporated with Nkx6.1 alone (Fig. 9A,B). Co-expression of RNF220 together with Nkx6.1 further promoted the activity of Nkx6.1 in inducing Chx10⁺ cells by ~157% and the activity of Gata3⁺ cells by ~140% compared with the control side (Fig. 9A,B). Strikingly, when RNF220 and ZC4H2 were overexpressed together with Nkx6.1, Chx10⁺ V2a INs and Gata3⁺ V2b INs were dramatically increased up to ~198% and ~178% compared with the control side (Fig. 9A,B). These results suggest that RNF220 likely functions together with ZC4H2 and Nkx6.1 to facilitate development of p2 and V2 INs. Next, we examined whether RNF220 mutants (Δ N) and ZC4H2 mutants (V63L, R198Q) that are defective in binding each other and degrading target proteins, lose the ability to promote Nkx6.1 to induce ectopic Chx10 expression in the chick neural tube. Indeed, the expression of these mutants, together with Nkx6.1, was not able to induce ectopic Chx10 expression compared with the WT RNF220 and ZC4H2 (Fig. S5).

DISCUSSION

The ventral patterning of the neural tube depends on the actions of extracellular signaling molecules such as Shh and a set of distinct transcription factors expressed by different types of neural progenitor cells. As neural progenitors differentiate into specific neurons during development, the appropriate level of key regulatory proteins is tightly controlled not only by *de novo* expression, but also by selective removal of erroneously expressed proteins. Although the molecular mechanisms of neuronal cell fate determination at the level of gene regulation have been relatively well documented, the regulation of protein abundance through protein degradation via the

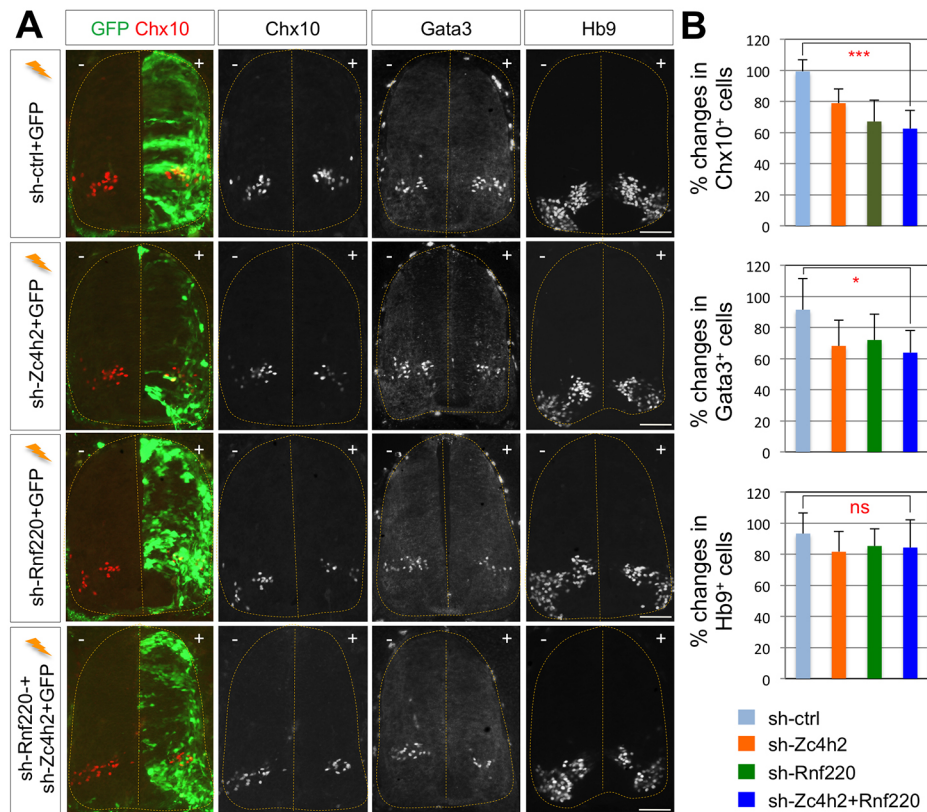


Fig. 8. RNF220 and ZC4H2 are required for the generation of V2 INs. (A) *In ovo* electroporation of sh-control, sh-Zc4h2, sh-Rnf220 or sh-Rnf220+sh-Zc4h2 with GFP was performed at HH13, followed by immunostaining analyses with indicated antibodies for chick embryos (thoracic level). Knockdown of RNF220 and ZC4H2 in developing chick embryos decreased the number of Chx10⁺ V2a INs and Gata3⁺ V2b INs compared with the non-electroporated control side. Yellow dotted lines indicate the outline of the spinal cord. +, electroporated side; -, non-electroporated side. (B) Quantification of Chx10⁺, Gata3⁺ or Hb9⁺ neurons in the electroporated side relative to those in the unelectroporated side. Data are mean±s.d. **P*<0.05, ****P*<0.001 (Student's *t*-test); ns, not significant. Scale bars: 100μm.

ubiquitin/proteasome pathway in developing embryos remains relatively poorly understood (Saritas-Yildirim and Silva, 2014). In this report, we present our findings that support the vital roles of RNF220 in the patterning of the ventral progenitor domains, at least in part through modulating the levels of Dbx, Irx3, FoxN4 and Nkx proteins (Fig. 10). First, RNF220 and ZC4H2 are expressed in ventral progenitor domains of the spinal cord (Fig. 1) and regulate each other's protein levels (Fig. 2). Second, deletion of *Rnf220* in mice results in abnormal ventral progenitor formation, including loss of the p2 progenitor domain, reduction of the p1 and pMN progenitor domains, ventral expansion of the p0 progenitor domain and dorsal expansion of the p3 progenitor domain (Figs 6 and 10), ultimately leading to the complete loss of V2 INs, the reduction of V1 INs and MNs, and the increase of V0 INs and V3 INs (Figs 7 and 10). Changes in the protein levels of Irx3, FoxN4 and Nkx6.1 by RNF220/ZC4H2 may result in the loss of the p2 domain and V2 INs in *Rnf220* mutant embryos. Notably, in chick electroporation, we observed that simultaneous knockdown of both RNF220 and ZC4H2 resulted in a significant decrease in V2 INs but no difference in MNs (Fig. 8). We think the lack of MN loss in chick experiments is likely due to the less-than-optimal knockdown efficiency of RNF220 and ZC4H2 (Fig. S4). Interestingly, RNF220 and ZC4H2 appear to potentiate the activity of Nkx6.1 in inducing V2 INs, as shown by an increase in Chx10⁺ and Gata3⁺ V2 INs by overexpressed Nkx6.1 together with RNF220 and ZC4H2 (Fig. 9), and a decrease in V2 INs by knockdown of RNF220 and ZC4H2 in the developing spinal cord (Fig. 8). However, RNF220 may also have additional target substrates expressed in the p2 or pMN domains, which play important roles in patterning and/or function of the p2 or pMN domains. Identification of such RNF220 substrates would be an interesting future study. Finally, RNF220 and ZC4H2 mediate the ubiquitylation and proteasomal degradation of Dbx and

other proteins, which is likely to limit the borders of ventral progenitor domains (Fig. 3 and Fig. S2). Altered Dbx2 degradation may lead to changes in the p2, p3 and pMN domains and increased Dbx1 may result in expansion of p0. Irx3 changes can also contribute to alterations in p1 and p0. Similarly, altered degradation of Nkx2.2 can explain p3 domain expansion, and impaired Nkx6.1 degradation may be responsible for p3, pMN and p2 alterations. These findings demonstrate that RNF220 and ZC4H2 associate with each other and function together to properly refine the distinct borders of ventral progenitor domains through degrading a specific set of factors that are involved in the patterning of neighboring cell populations.

Ubiquitin/proteasome pathways have been reported to play crucial roles in neural progenitor cell maintenance and neurogenesis during embryonic development. The ubiquitin ligase mLin41 is expressed in neural progenitor cells and promotes FGF signaling by directly binding to and enhancing the stability of Shc SH2-binding protein 1 (SHCBP1), an important component of the FGF signaling pathway that maintains neural progenitor cells (Chen et al., 2012). Ubiquitin ligase can also play an important role in modulating various signaling pathways by adding a ubiquitin moiety to the target protein for downstream signal transduction, without degrading target proteins. For example, mind bomb 1 (Mib1) is an E3 ubiquitin ligase that ubiquitylates delta and promotes its internalization, which is essential for activation of notch signaling by delta, demonstrating that Mib1 has a primary role in protein trafficking, not target protein degradation (Itoh et al., 2003). Modulation of delta-notch signaling by Mib1 is also involved in the control of neurogenesis and gliogenesis in the developing spinal cord (Kang et al., 2013). *Mib1* deletion in mice results in the depletion of spinal progenitors, premature neuronal differentiation and unbalanced specification of V2 INs, which mimic the notch phenotype (Kang et al., 2013). Our results in this study uncover a new role for a protein degradation pathway in neural

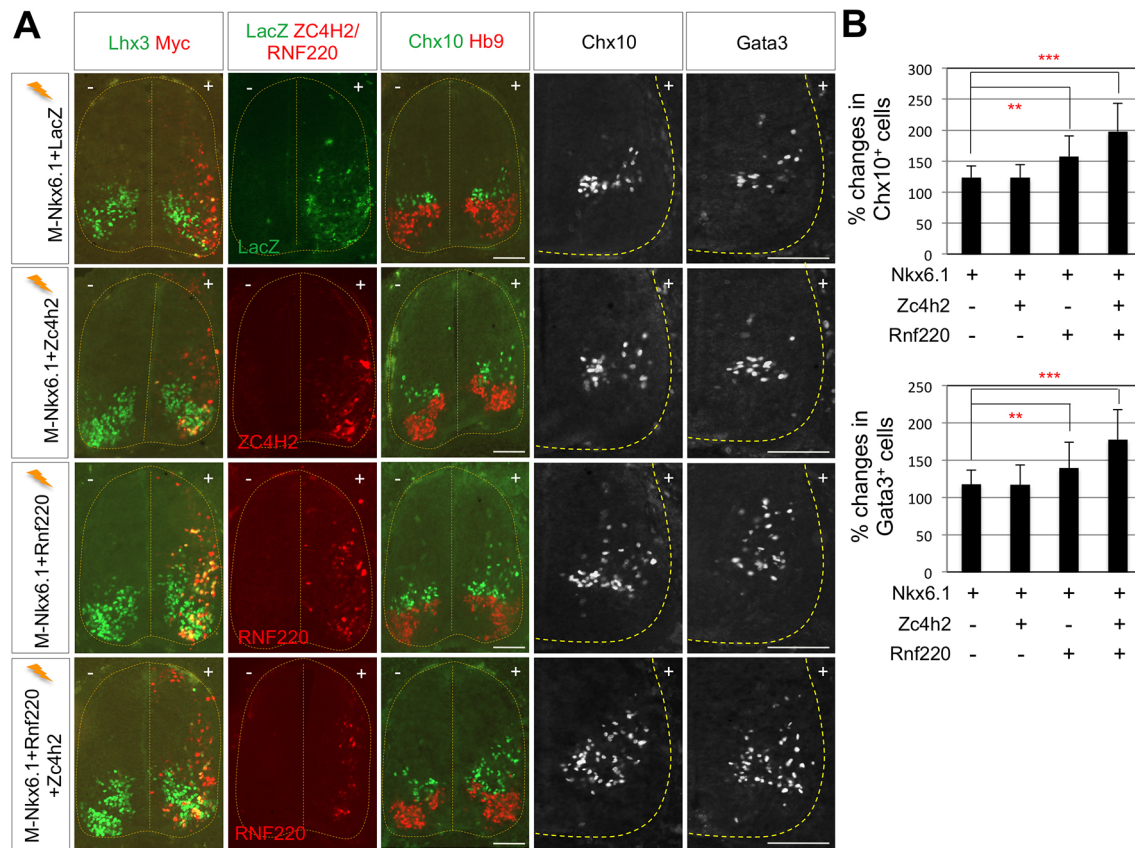


Fig. 9. Ectopic induction of V2 INs by co-expression of RNF220 and ZC4H2 together with Nkx6.1. (A) Immunostaining analyses with indicated antibodies (to visualize Chx10, Gata3, Hb9, Myc, RNF220, ZC4H2 and *lacZ*) for chick embryos electroporated with Myc-Nkx6.1+*lacZ*, Myc-Nkx6.1+Zc4h2, Myc-Nkx6.1+Rnf220 and Myc-Nkx6.1+Rnf220+Zc4h2 (thoracic level). Co-expression of RNF220 and ZC4H2 together with Nkx6.1 increased the number of Chx10⁺ V2a INs and Gata3⁺ V2b INs in the electroporated side of the spinal cord (dotted lines). +, electroporated side; -, non-electroporated side. (B) Quantification of Chx10⁺ or Gata3⁺ neurons in the electroporated side relative to those in the non-electroporated side of chick neural tube. Data are mean±s.d. ** $P < 0.01$, *** $P < 0.001$ (Student's *t*-test). Scale bars: 100µm.

progenitor fate specification, expanding the repertoire of ubiquitin/proteasome pathways in embryonic development.

Notably, the influence of RNF220 on the stability of ZC4H2 or other substrates appears to be subtle in cultured cells. Given our results showing much greater impact *in vivo* and the drastic consequences on progenitor domains in *Rnf220* mutants, we argue that other factors, which are present during embryogenesis but not in cultured cells, may be required for effective degradation of our newly defined factors in progenitor domains by RNF220. Further studies on this issue, such as discovery of additional effectors of RNF220-directed degradation present in embryos, will provide crucial insights into the regulatory mechanism by which the protein levels are maintained appropriately during early development and organogenesis.

Mutations in ZC4H2 in humans result in rare X-linked neurodevelopmental disorders WS/AMC/MCS. In males, severe intellectual disability is associated with various symptoms such as muscle weakness, severe joint contractures, delayed motor development, seizures and other central nervous system abnormalities (Hirata et al., 2013; May et al., 2015). Most females show no deficits at all, as most mutations in ZC4H2 reside in the inactivated X-chromosome (Hirata et al., 2013). However, some females with heterozygous mutations in ZC4H2 can also be affected, although to a lesser degree, showing mild features of the disorder (Hirata et al., 2013). Also it has recently been reported that a female carrying a ZC4H2 deletion showed severe neurodevelopmental

impairment (Zanzottera et al., 2017), suggesting that the phenotypic analysis of a full spectrum of ZC4H2 variants is still incomplete. Our results in this report indicating a cooperative action of RNF220 and ZC4H2 in the generation of spinal progenitor domains may underlie the missing etiology for at least some symptoms of WS/AMC/MCS. For example, it is possible that delayed motor development and muscle weakness in WS/AMC/MCS patients may involve deficits in motor circuitry caused by a decrease in V2 INs and MNs as well as alterations in other INs, which involve RNF220, although we cannot exclude the possibility that these symptoms of WS/AMC/MCS can alternatively result from RNF220-independent events or both RNF220-dependent and independent pathways. In this regard, it is interesting to note that, although WS/AMC/MCS are X-linked recessive disorders, which mainly affect males, we have not observed any sexual dimorphism in the spinal phenotypes of *Rnf220*^{-/-} embryos. Most *Rnf220*^{-/-} mice died as embryos; however, some *Rnf220*^{-/-} pups died immediately after birth. In contrast, *Rnf220*^{+/-} mice were born without any apparent phenotype, such as an abnormal walking pattern or impaired motor skills. It is also noted that mutations in RNF220 have not yet been reported to cause WS/AMC/MCS. Taken together, these results suggest that RNF220 homozygous mutations in humans are likely to be lethal, whereas RNF220 heterozygous mutations are asymptomatic. However, WS/AMC/MCS are relatively new disorders, and it remains to be seen whether all WS/AMC/MCS patients carry mutations only in ZC4H2, and not in RNF220.

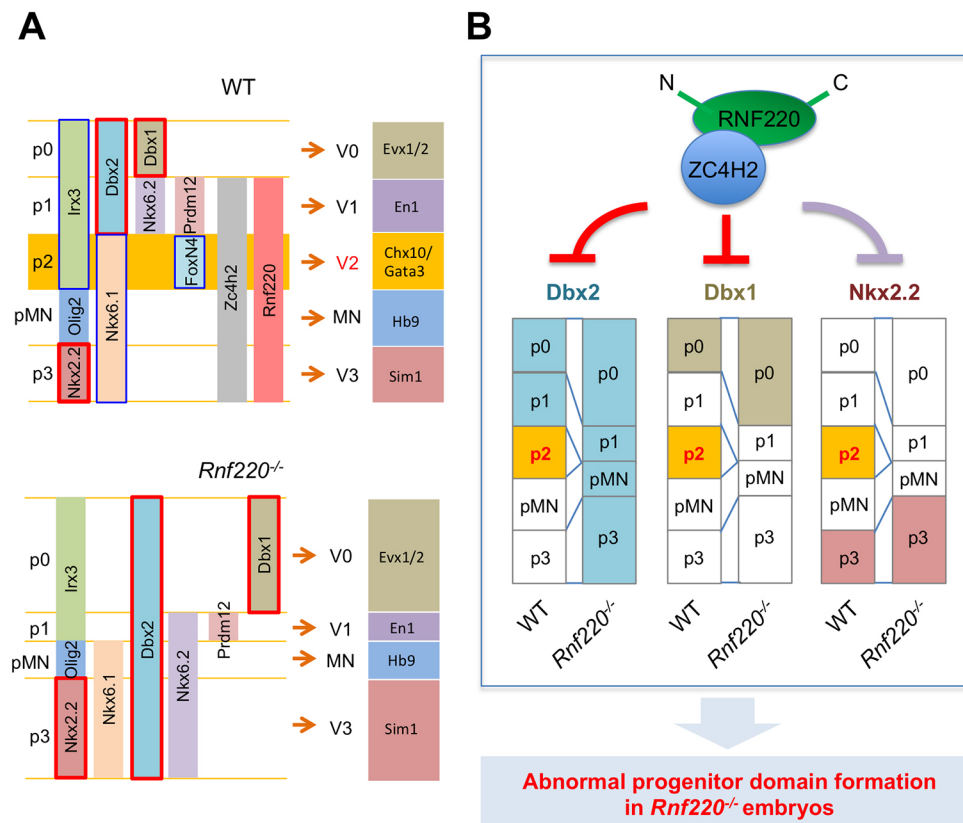


Fig. 10. Working model of RNF220 in the patterning of ventral progenitor domains. (A) Summary describing the change of expression pattern of class I and II transcription factors in the spinal cord of *Rnf220*^{-/-} embryos compared with that of WT mouse spinal cords. (B) RNF220 together with ZC4H2 represses or limits the boundaries of the ventral spinal neuronal cell identities through degradation of proteins such as Dbx1/2 and Nkx2.2. The absence of *Rnf220* causes irregular induction or stabilization of Dbx1/2 and Nkx2.2 transcription factors, which results in abnormal progenitor domain formation in *Rnf220*^{-/-} embryos.

Interestingly, out of several point mutations in *ZC4H2* that have been found in AMC patients, V63L, R198Q and P201S were shown to cause a decrease in synapse number and density in primary mouse hippocampal neurons (Hirata et al., 2013). Although we found that V63L and R198Q mutants failed to stabilize RNF220 and to degrade Dbx2 (Fig. S3), and therefore the V63 and R198 residues of *ZC4H2* are likely to be important for the reported role of *ZC4H2* in the formation of the p2 progenitor domain and V2 IN generation (Fig. S5) (May et al., 2015), it remains to be determined whether RNF220 is also required for *ZC4H2* to facilitate synapse formation in hippocampal neurons.

In summary, we showed that RNF220 plays crucial roles in the patterning of the ventral progenitor domains, by targeting multiple transcription factors, including Dbx1/2 and Nkx2.2, for degradation in close cooperation with *ZC4H2*, which is encoded by the WS/AMC/MCS gene *ZC4H2* in humans. Both RNF220 and *ZC4H2* are also expressed in differentiated neurons (Figs 2E and 7A), and it will be interesting to investigate whether they play important roles in mature neurons as well. Finally, our identification of an E3 ubiquitin ligase enzyme in the generation of progenitor domains may provide a new therapeutic target for treating various neurodevelopmental disorders, and contribute to engineering stem cells toward specific neuronal types, a desirable feature in cell therapy.

MATERIALS AND METHODS

DNA constructs

Human *RNF220* full length, *RNF220* deletion constructs, and human *ZC4H2*, mouse *Dbx1*, zebrafish *dbx2* and *nkx6.1* were cloned into pCS2 and/or pcDNA4 containing a HA-, Flag-, Myc- or His-epitope tag for expression in mammalian cells and chick embryos, as previously described (Lee et al., 2012, 2004; Lee and Pfaff, 2003). Mutations in human *RNF220* and *ZC4H2* were introduced using a PCR-based mutagenesis method and verified by sequencing. Human *ZC4H2* was cloned into a pEBG vector for glutathione-

S-transferase (GST) fusion protein expression. HA-tagged *RNF220* was cloned into an EF1 α vector for expression in the chick neural tube. For knockdown of *Rnf220* and *Zc4h2* in chick embryos, shRNA constructs against *Rnf220* and *Zc4h2* were prepared in a pSilencer vector. The shRNA-targeting sequences were as follows: 5'-TGCATGGACTCCTACACAA-3' for sh-*Rnf220*, and 5'-CTGTTTATCCTGTACACAA-3' for sh-*Zc4h2*.

In ovo electroporation, IHC and ISH assays

In ovo electroporation was performed as described (Thaler et al., 2002). Briefly, DNAs were injected into the lumen of the neural tube of Hamburger–Hamilton stage (HH) 13 chick embryos, which were then electroporated. The embryos were harvested 3 days post-electroporation and fixed in 4% paraformaldehyde, embedded in optimal cutting temperature compound and cryosectioned at 12 μ m thickness for IHC assays, or at 18 μ m thickness for ISH with digoxigenin-labeled probes. Each set of chick electroporation experiments was repeated independently at least three times, with three to six embryos injected with the same combination of plasmids at each experimental set. Cervical and thoracic levels of the chick embryo were used for ISH and IHC. Representative sets of images from reproducible results were presented.

For IHC assays, the following antibodies were used: mouse anti-Nkx6.1 [Developmental Studies Hybridoma Bank (DSHB), F55A10, 1:500], mouse anti-Pax6 (DSHB, PAX6, 1:500), rabbit anti-Olig2 (Abcam, ab15328, 1:1000), mouse anti-Nkx2.2 (DSHB, 74.5A5, 1:500), rabbit anti-Sox2 (Abcam, ab97959, 1:1000), mouse anti-TuJ1 (Covance, MMS-435P, 1:5000), mouse anti-Hb9/MNR2 (DSHB, 5C10, 1:500), guinea pig anti-Hb9 (homemade), guinea pig anti-Chx10 (homemade), rabbit anti-Gata3 (homemade), guinea pig anti-Sox14 (homemade), rabbit anti-Lhx3 (Abcam, ab14555, 1:500), rabbit anti-Rnf220 (Novus Biologicals, NBP1-88487, 1:2500), rabbit anti-Zc4h2 (Novus Biologicals, NBP2-13538, 1:2500), chicken anti- β -gal (Abcam, ab9361, 1:5000), mouse anti-Myc (Millipore, 9E10, 1:5000) and mouse anti-HA (Covance, MMS-101R, 1:5000). Antigen regions for homemade antibodies were 234-403aa of rat Hb9, 1-154aa of mouse Chx10, 1-221aa of mouse Gata3 and 1-240aa of mouse Sox14. Antigenic proteins were induced in 0.5 mM isopropyl

β -D-1-thiogalactopyranoside at 37°C for 6 h. Induced proteins were isolated from the SDS-PAGE gel and injected into rabbit or guinea pig, following the standard protocol for antibody production (Jackson and Fox, 1995). Antibodies were validated using western blotting.

For ISH analyses, cDNAs for mouse *Dbx1*, *En1*, *Sim1* and *Rnf220* were cloned to a pBluescript vector to generate digoxigenin-labeled riboprobes. For fluorescence *in situ* hybridization, *Rnf220* riboprobe was generated with 10 \times fluorescein RNA labeling mix (BMC, 1685619) and *Dbx1* riboprobe was generated with 10 \times DIG RNA labeling mix (BMB, 1277073). FITC-labeled RNF220 was detected using anti-FITC-POD antibody (Roche, 1426346, 1:500) with FITC-Tyramide (TSA Plus Fluorescein Fluorescence System) (PerkinElmer, NEL741) and DIG-labeled *Dbx1* was detected using anti-digoxigenin-POD antibody (Roche, 11207733910, 1:500) with Cy5-Tyramide (TSA Plus Cy5 Fluorescence System) (PerkinElmer, NEL745). cDNAs for mouse *Nkx6.2* (#15542, deposited by John Rubenstein) and *Dbx2* (#16288, deposited by Thomas Jessell) were purchased from Addgene and used to generate digoxigenin-labeled riboprobes.

Mice

All mouse experiments were performed under an approved protocol by the Institutional Animal Care and Use Committee of the Seoul National University. *Rnf220* mice were generated using the CRISPR/Cas9 system, with an sgRNA that targets exon7 of the *Rnf220* gene, producing a mouse line with 17 nucleotides deleted (Fig. 5A). Targeted *Rnf220* produces a fragmented protein of RNF220 (1-384aa). But this C-terminally deleted RNF220 fragment in the *Rnf220* KO was not detected in immunostaining with the anti-RNF220 antibody that recognizes a region including 44-145aa of RNF220, suggesting that the transcript of *Rnf220* from the mutant allele was not stable enough to be translated, or that the translated protein was unstable and so it degraded. It was confirmed that no RNF220 protein was expressed by immunostaining with RNF220 antibody. Targeting sgRNA was 5'-TCAGGCGCTCCAGCTCAGAGAGG-3'; genotyping primers were *Rnf220*-FP: 5'-GGACAGCAACCGCTTTGAGG-3' and *Rnf220*-RP: 5'-ACCCAAGTTGTCTCAGTCTT-3', which produces 108 bp for the WT allele and 91 bp for the KO allele. *Rnf220*^{+/-} male mice were crossed with *Rnf220*^{+/-} female mice to get KO mutant embryos for the analyses. Mouse embryos were collected at indicated developmental stages, and processed similarly to chick embryos as described above. Cervical, brachial and thoracic levels of the mouse embryo were used for ISH and IHC. For the quantification, at least four independent litters were analyzed for each embryonic stage and cell number was counted from more than 20 images of four to five embryos of WT and *Rnf220*^{+/-}.

Image analysis and quantification

A Zeiss Axio imager was used to image ISH and IHC results. Integrated density measurement in ImageJ software was carried out to analyze intensity. Statistical differences were determined using Student's *t*-test. Statistical significance is displayed as **P*<0.05, ***P*<0.01, ****P*<0.001 or *****P*<0.0001. Not significant is indicated by 'ns' (*P*>0.05).

Co-immunoprecipitation assays and immunoblotting assays

HEK293T cells were cultured in DMEM media supplemented with 10% fetal bovine serum (FBS). For co-immunoprecipitation, HEK293T cells were seeded on 10 cm tissue culture dishes, cultured in DMEM media supplemented with 10% FBS and transfected with the expression vectors for HA-RNF220, Flag-ZC4H2 and Myc-Dbx2, using Superfect (Qiagen). Cells were harvested and lysed in IP buffer [20 mM Tris-HCl (pH 8.0), 0.5% NP-40, 1 mM EDTA, 150 mM NaCl, 2 mM PMSF, 10% glycerol, 4 mM Na₃VO₄, 200 mM NaF, 20 mM Na-pyrophosphate and protease inhibitor cocktail] 2 days after transfection. In these studies, immunoprecipitations were performed with mouse anti-Myc (Millipore, 1 μ g) or mouse anti-Flag (Sigma-Aldrich, F3165, 1 μ g) antibodies. The interactions were monitored by western blotting assays using mouse anti-HA (Covance, 1:5000), mouse anti-Flag (Sigma-Aldrich, 1:5000) and mouse anti-Myc (Millipore, 1:5000) antibodies. At least three independent experiments were used for the quantification. Integrated density measurement in ImageJ software was carried out to analyze densitometry.

In vivo GST pull-down assay

For the cell-based GST pull-down assay, HEK293T cells were transfected with HA-RNF220 and Myc-DBX2, together with GST-ZC4H2 or GST. After 48 h, cells were lysed and incubated with glutathione-sepharose 4B beads. Samples were eluted by boiling, and visualized by blotting with mouse anti-HA (Covance, 1:5000), mouse anti-Myc (Millipore, 1:5000) and mouse anti-GST (Santa Cruz Biotechnology, SC-138, 1:1000) antibodies.

In vivo ubiquitylation assay

HEK293T cells were transfected with HA-Ubiquitin, Myc-Dbx2 and His-Rnf220 as indicated. Cells were treated with 1 μ M MG132 for 24 h before harvest and then lysed and immunoprecipitated with mouse anti-Myc antibody (Millipore, 1 μ g). Inputs from total cell lysate and eluted proteins were then detected with HA or Myc antibodies.

Acknowledgements

We thank Dr Soo-Kyung Lee (Oregon Health & Science University, Portland, USA) for reagents and many helpful suggestions during the course of this work, and Dr Soo-Kyung Lee and Dr Jae W. Lee (Oregon Health & Science University, Portland, USA) for critically reading the manuscript.

Competing interests

The authors declare no competing or financial interests.

Author contributions

Conceptualization: S.L.; Methodology: J.K.; Validation: J.K., T.-I.C., S.P., M.H.K.; Formal analysis: J.K.; Investigation: S.L.; Resources: T.-I.C., C.-H.K.; Data curation: S.L.; Writing-original draft: J.K., S.L.; Writing - review & editing: S.L.; Supervision: S.L.; Funding acquisition: C.-H.K., S.L.

Funding

This research was supported by a National Research Foundation of Korea grant, funded by the Ministry of Science, ICT and Future Planning [2017R1A2B2010696 to C.-H.K.] and a grant from the Korea Health Technology R&D Project via the Korea Health Industry Development Institute, funded by the Ministry of Health and Welfare, Republic of Korea [HI17C0447 to S.L.].

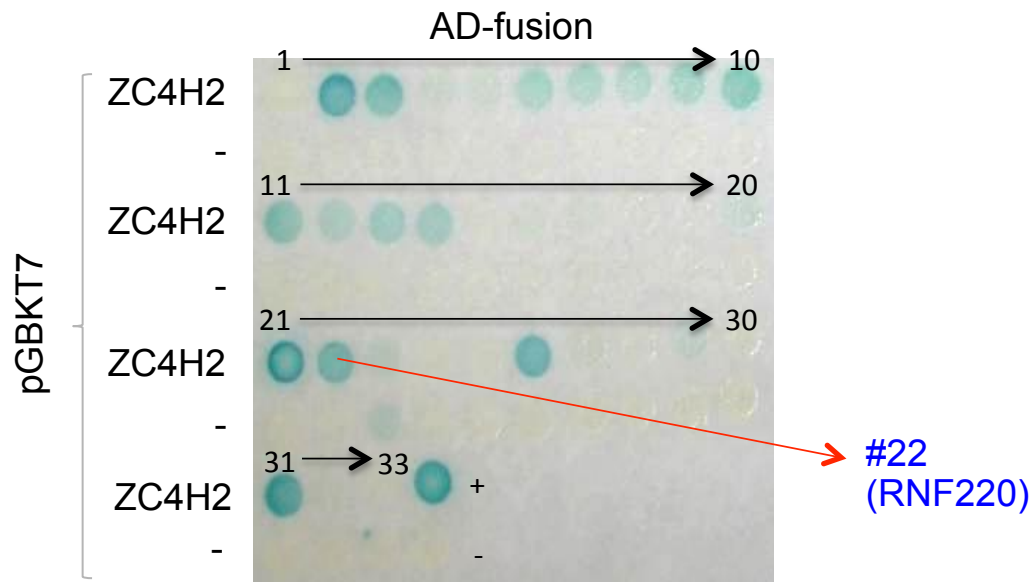
Supplementary information

Supplementary information available online at <http://dev.biologists.org/lookup/doi/10.1242/dev.165340.supplemental>

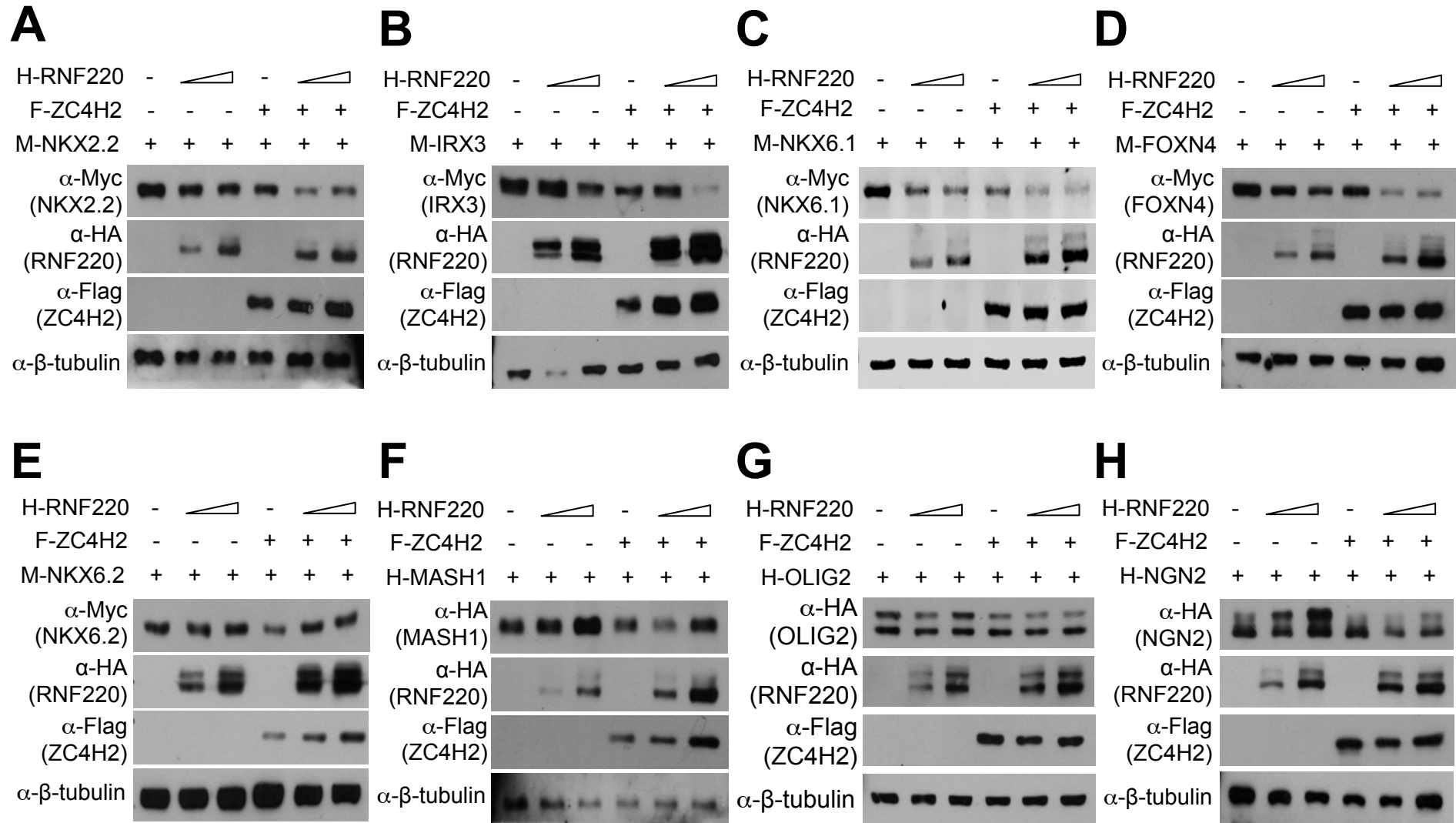
References

- Al-Mosawie, A., Wilson, J. M. and Brownstone, R. M. (2007). Heterogeneity of V2-derived interneurons in the adult mouse spinal cord. *Eur. J. Neurosci.* **26**, 3003-3015.
- Borowska, J., Jones, C. T., Zhang, H., Blacklaws, J., Goulding, M. and Zhang, Y. (2013). Functional subpopulations of V3 interneurons in the mature mouse spinal cord. *J. Neurosci.* **33**, 18553-18565.
- Briscoe, J. and Ericson, J. (1999). The specification of neuronal identity by graded Sonic Hedgehog signalling. *Semin. Cell Dev. Biol.* **10**, 353-362.
- Briscoe, J., Pierani, A., Jessell, T. M. and Ericson, J. (2000). A homeodomain protein code specifies progenitor cell identity and neuronal fate in the ventral neural tube. *Cell* **101**, 435-445.
- Burrill, J. D., Moran, L., Goulding, M. D. and Saueressig, H. (1997). PAX2 is expressed in multiple spinal cord interneurons, including a population of EN1+ interneurons that require PAX6 for their development. *Development* **124**, 4493-4503.
- Chen, J., Lai, F. and Niswander, L. (2012). The ubiquitin ligase mLin41 temporally promotes neural progenitor cell maintenance through FGF signaling. *Genes Dev.* **26**, 803-815.
- Clovis, Y. M., Seo, S. Y., Kwon, J.-S., Rhee, J. C., Yeo, S., Lee, J. W., Lee, S. and Lee, S.-K. (2016). Chx10 consolidates V2a interneuron identity through two distinct gene repression modes. *Cell Reports* **16**, 1642-1652.
- Del Barrio, M. G., Taveira-Marques, R., Muroyama, Y., Yuk, D.-I., Li, S., Wines-Samuels, M., Shen, J., Smith, H. K., Xiang, M., Rowitch, D. et al. (2007). A regulatory network involving Foxn4, Mash1 and delta-like 4/Notch1 generates V2a and V2b spinal interneurons from a common progenitor pool. *Development* **134**, 3427-3436.
- Ericson, J., Muhr, J., Jessell, T. M. and Edlund, T. (1995). Sonic hedgehog: a common signal for ventral patterning along the rostrocaudal axis of the neural tube. *Int. J. Dev. Biol.* **39**, 809-816.
- Ericson, J., Briscoe, J., Rashbass, P., van Heyningen, V. and Jessell, T. M. (1997a). Graded sonic hedgehog signaling and the specification of cell fate in the ventral neural tube. *Cold Spring Harbor Symp. Quant. Biol.* **62**, 451-466.

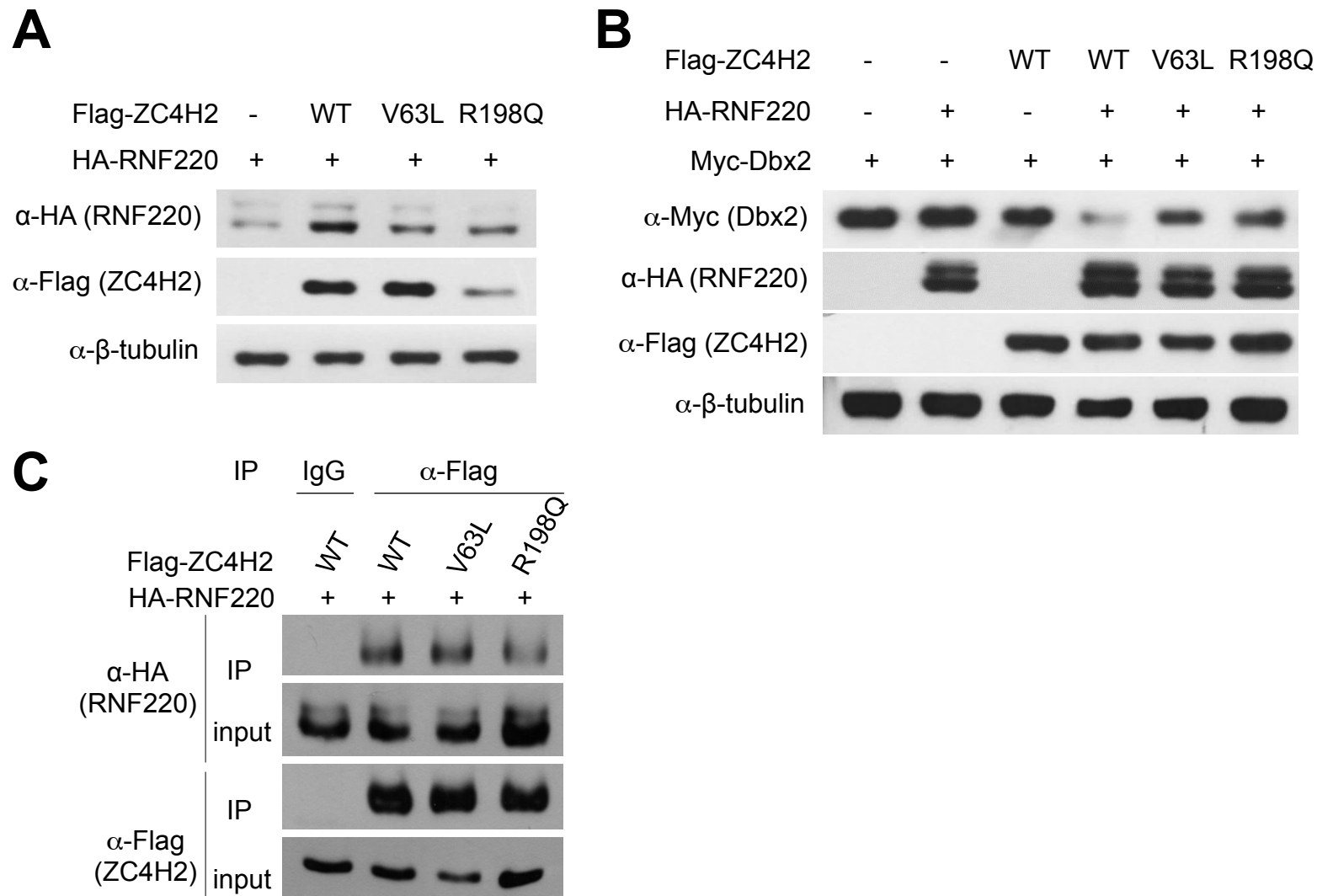
- Ericson, J., Rashbass, P., Schedl, A., Brenner-Morton, S., Kawakami, A., van Heyningen, V., Jessell, T. M. and Briscoe, J. (1997b). Pax6 controls progenitor cell identity and neuronal fate in response to graded Shh signaling. *Cell* **90**, 169-180.
- Francius, C., Ravassard, P., Hidalgo-Figueroa, M., Mallet, J., Clotman, F. and Nardelli, J. (2015). Genetic dissection of Gata2 selective functions during specification of V2 interneurons in the developing spinal cord. *Dev. Neurobiol.* **75**, 721-737.
- Goulding, M. and Lamar, E. (2000). Neuronal patterning: making stripes in the spinal cord. *Curr. Biol.* **10**, R565-R568.
- Hargrave, M., Karunaratne, A., Cox, L., Wood, S., Koopman, P. and Yamada, T. (2000). The HMG box transcription factor gene Sox14 marks a novel subset of ventral interneurons and is regulated by sonic hedgehog. *Dev. Biol.* **219**, 142-153.
- Hirata, H., Nanda, I., van Riesen, A., McMichael, G., Hu, H., Hambrock, M., Papon, M.-A., Fischer, U., Marouillat, S., Ding, C. et al. (2013). ZC4H2 mutations are associated with arthrogryposis multiplex congenita and intellectual disability through impairment of central and peripheral synaptic plasticity. *Am. J. Hum. Genet.* **92**, 681-695.
- Itoh, M., Kim, C.-H., Palardy, G., Oda, T., Jiang, Y.-J., Maust, D., Yeo, S.-Y., Lorick, K., Wright, G. J., Ariza-McNaughton, L. et al. (2003). Mind bomb is a ubiquitin ligase that is essential for efficient activation of Notch signaling by Delta. *Dev. Cell* **4**, 67-82.
- Jackson, L. R. and Fox, J. (1995). Institutional Policies and Guidelines on Adjuvants and Antibody Production. *ILAR Journal* **37**, 141-152.
- Jessell, T. M. (2000). Neuronal specification in the spinal cord: inductive signals and transcriptional codes. *Nat. Rev. Genet.* **1**, 20-29.
- Jinek, M., Chylinski, K., Fonfara, I., Hauer, M., Doudna, J. A. and Charpentier, E. (2012). A programmable dual-RNA-guided DNA endonuclease in adaptive bacterial immunity. *Science* **337**, 816-821.
- Jurata, L. W., Pfaff, S. L. and Gill, G. N. (1998). The nuclear LIM domain interactor NLI mediates homo- and heterodimerization of LIM domain transcription factors. *J. Biol. Chem.* **273**, 3152-3157.
- Kang, K., Lee, D., Hong, S., Park, S.-G. and Song, M.-R. (2013). The E3 ligase Mind bomb-1 (Mib1) modulates Delta-Notch signaling to control neurogenesis and gliogenesis in the developing spinal cord. *J. Biol. Chem.* **288**, 2580-2592.
- Kloos, D.-U., Jakubiczka, S., Wienker, T., Wolff, G. and Wieacker, P. (1997). Localization of the gene for Wieacker-Wolff syndrome in the pericentromeric region of the X chromosome. *Hum. Genet.* **100**, 426-430.
- Kong, Q., Zeng, W., Wu, J., Hu, W., Li, C. and Mao, B. (2010). RNF220, an E3 ubiquitin ligase that targets Sin3B for ubiquitination. *Biochem. Biophys. Res. Commun.* **393**, 708-713.
- Lee, S.-K. and Pfaff, S. L. (2003). Synchronization of neurogenesis and motor neuron specification by direct coupling of bHLH and homeodomain transcription factors. *Neuron* **38**, 731-745.
- Lee, S.-K., Jurata, L. W., Funahashi, J., Ruiz, E. C. and Pfaff, S. L. (2004). Analysis of embryonic motoneuron gene regulation: derepression of general activators function in concert with enhancer factors. *Development* **131**, 3295-3306.
- Lee, S.-K., Lee, B., Ruiz, E. C. and Pfaff, S. L. (2005). Olig2 and Ngn2 function in opposition to modulate gene expression in motor neuron progenitor cells. *Genes Dev.* **19**, 282-294.
- Lee, S., Cuvillier, J. M., Lee, B., Shen, R., Lee, J. W. and Lee, S.-K. (2012). Fusion protein Isl1-Lhx3 specifies motor neuron fate by inducing motor neuron genes and concomitantly suppressing the interneuron programs. *Proc. Natl. Acad. Sci. USA* **109**, 3383-3388.
- Li, S., Misra, K., Matisse, M. P. and Xiang, M. (2005). Foxn4 acts synergistically with Mash1 to specify subtype identity of V2 interneurons in the spinal cord. *Proc. Natl. Acad. Sci. USA* **102**, 10688-10693.
- Ma, P., Yang, X., Kong, Q., Li, C., Yang, S., Li, Y. and Mao, B. (2014). The ubiquitin ligase RNF220 enhances canonical Wnt signaling through USP7-mediated deubiquitination of beta-catenin. *Mol. Cell. Biol.* **34**, 4355-4366.
- May, M., Hwang, K. S., Miles, J., Williams, C., Niranjana, T., Kahler, S. G., Chiurazzi, P., Steindl, K., Van Der Spek, P. J., Swagemakers, S. et al. (2015). ZC4H2, an XLID gene, is required for the generation of a specific subset of CNS interneurons. *Hum. Mol. Genet.* **24**, 4848-4861.
- Muroyama, Y., Fujiwara, Y., Orkin, S. H. and Rowitch, D. H. (2005). Specification of astrocytes by bHLH protein SCL in a restricted region of the neural tube. *Nature* **438**, 360-363.
- Pierani, A., Brenner-Morton, S., Chiang, C. and Jessell, T. M. (1999). A sonic hedgehog-independent, retinoid-activated pathway of neurogenesis in the ventral spinal cord. *Cell* **97**, 903-915.
- Pierani, A., Moran-Rivard, L., Sunshine, M. J., Littman, D. R., Goulding, M. and Jessell, T. M. (2001). Control of interneuron fate in the developing spinal cord by the progenitor homeodomain protein Dbx1. *Neuron* **29**, 367-384.
- Qiu, M., Shimamura, K., Sussel, L., Chen, S. and Rubenstein, J. L. R. (1998). Control of anteroposterior and dorsoventral domains of Nkx-6.1 gene expression relative to other Nkx genes during vertebrate CNS development. *Mech. Dev.* **72**, 77-88.
- Ran, F. A., Hsu, P. D., Wright, J., Agarwala, V., Scott, D. A. and Zhang, F. (2013). Genome engineering using the CRISPR-Cas9 system. *Nat. Protoc.* **8**, 2281-2308.
- Ravanelli, A. M. and Appel, B. (2015). Motor neurons and oligodendrocytes arise from distinct cell lineages by progenitor recruitment. *Genes Dev.* **29**, 2504-2515.
- Roelink, H., Porter, J. A., Chiang, C., Tanabe, Y., Chang, D. T., Beachy, P. A. and Jessell, T. M. (1995). Floor plate and motor neuron induction by different concentrations of the amino-terminal cleavage product of sonic hedgehog autoproteolysis. *Cell* **81**, 445-455.
- Sander, M., Paydar, S., Ericson, J., Briscoe, J., Berber, E., German, M., Jessell, T. M. and Rubenstein, J. L. (2000). Ventral neural patterning by Nkx homeobox genes: Nkx6.1 controls somatic motor neuron and ventral interneuron fates. *Genes Dev.* **14**, 2134-2139.
- Saritas-Yildirim, B. and Silva, E. M. (2014). The role of targeted protein degradation in early neural development. *Genesis* **52**, 287-299.
- Sun, T., Dong, H., Wu, L., Kane, M., Rowitch, D. H. and Stiles, C. D. (2003). Cross-repressive interaction of the Olig2 and Nkx2.2 transcription factors in developing neural tube associated with formation of a specific physical complex. *J. Neurosci.* **23**, 9547-9556.
- Thaler, J. P., Lee, S.-K., Jurata, L. W., Gill, G. N. and Pfaff, S. L. (2002). LIM factor Lhx3 contributes to the specification of motor neuron and interneuron identity through cell-type-specific protein-protein interactions. *Cell* **110**, 237-249.
- Vallstedt, A., Muhr, J., Pattyn, A., Pierani, A., Mendelsohn, M., Sander, M., Jessell, T. M. and Ericson, J. (2001). Different levels of repressor activity assign redundant and specific roles to Nkx6 genes in motor neuron and interneuron specification. *Neuron* **31**, 743-755.
- Yang, H., Wang, H. and Jaenisch, R. (2014). Generating genetically modified mice using CRISPR/Cas-mediated genome engineering. *Nat. Protoc.* **9**, 1956-1968.
- Zanzottera, C., Milani, D., Alfei, E., Rizzo, A., D'Arrigo, S., Esposito, S. and Pantaleoni, C. (2017). ZC4H2 deletions can cause severe phenotype in female carriers. *Am. J. Med. Genet. A* **173**, 1358-1363.
- Zhou, Q. and Anderson, D. J. (2002). The bHLH transcription factors OLIG2 and OLIG1 couple neuronal and glial subtype specification. *Cell* **109**, 61-73.



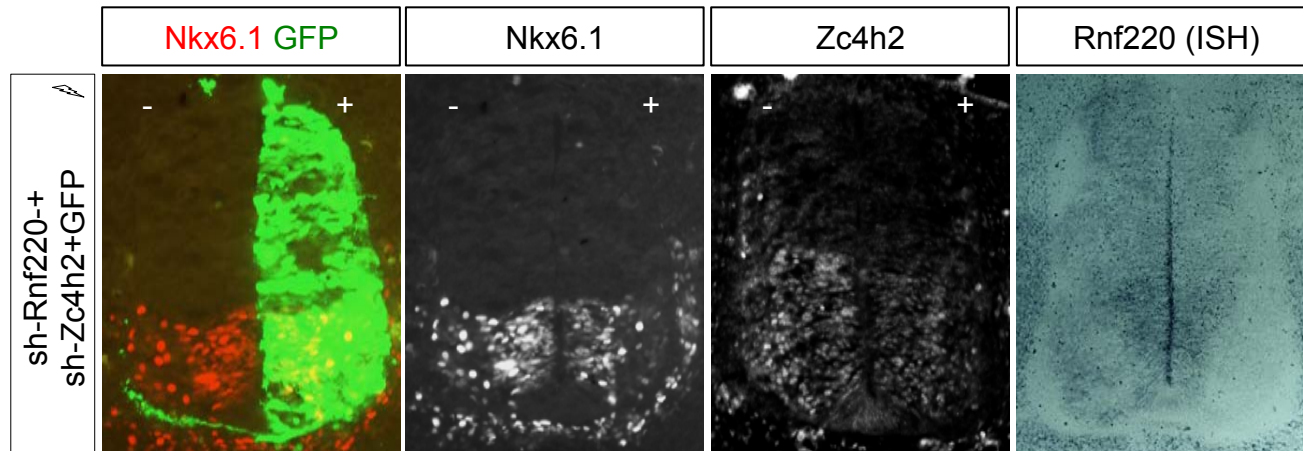
Supplementary Fig. 1: Identification of RNF220 as an interactor of ZC4H2. Interacting proteins with Gal4 fusion to ZC4H2 from our yeast two hybrid screening includes the RNF220.



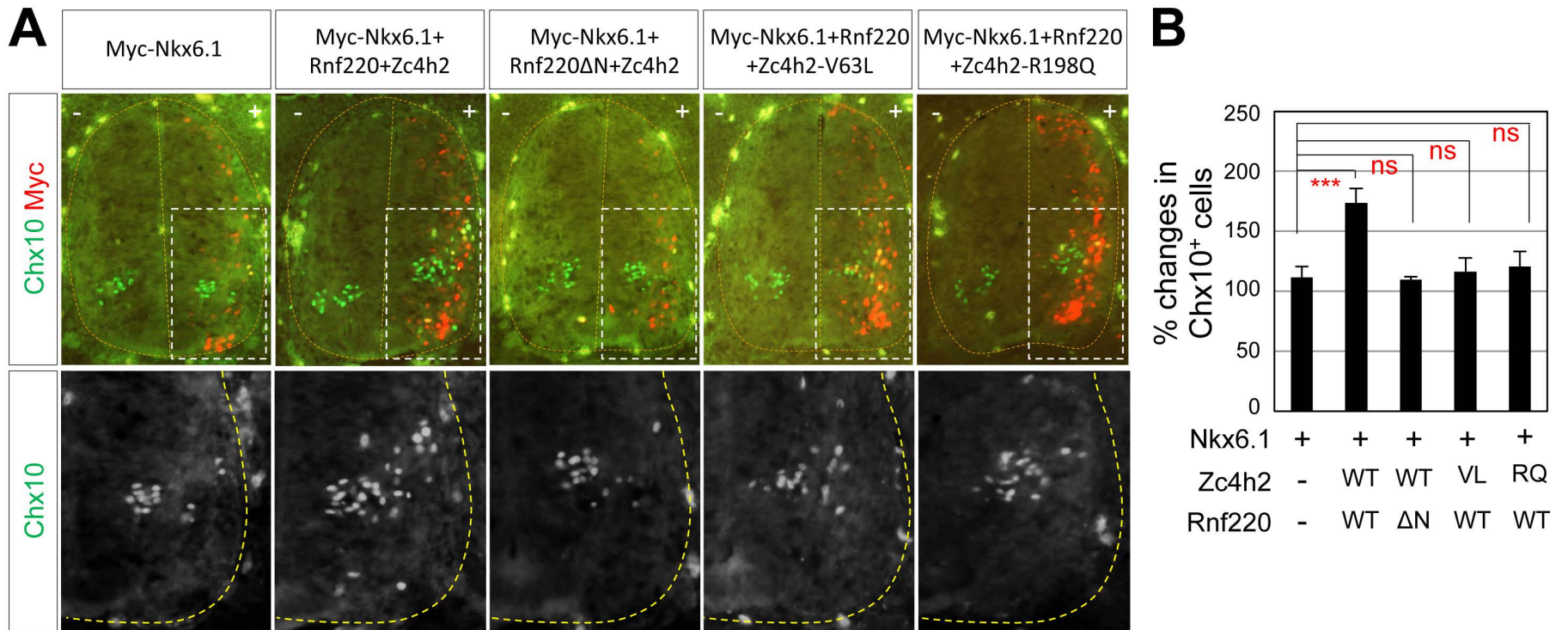
Supplementary Fig. 2: NKX2.2, IRX3, NKX6.1 and FOXN4 are degraded by RNF220 in the presence of ZC4H2. The protein levels of NKX2.2, IRX3, NKX6.1 and FOXN4 were reduced in the presence of RNF220/ZC4H2 in a dose-dependent manner but the levels of NKX6.2, MASH1, OLIG2 and NGN2 were not reduced by the presence of RNF220/ZC4H2.



Supplementary Fig. 3: ZC4H2 point mutants lose the ability to stabilize RNF220 and to degrade Dbx2 protein. (A) ZC4H2 V63L and R198Q mutants found in WRWF patients failed to stabilize RNF220 proteins, while ZC4H2 WT increased the protein level of RNF220. (B) ZC4H2 V63L and R198Q mutants were less effective in degrading Dbx2 protein compared to the WT ZC4H2 in the presence of RNF220. (C) The interaction between RNF220 and ZC4H2 R198Q mutant was reduced compared to ZC4H2 WT.



Supplementary Fig. 4: Reduced expression of Rnf220, Zc4h2 and Nkx6.1 in chick neural tube electroporated with sh-Rnf220 and sh-Zc4h2. GFP expression indicates the efficiency of the electroporation. In the knockdown constructs electroporated side (+), Zc4h2 and Rnf220 level was reduced and Nkx6.1 expression was also reduced marginally.



Supplementary Fig. 5: RNF220 mt (Δ N) and Zc4h2 mt (V63L, R198Q) lost the ability to promote Nkx6.1 to induce ectopic Chx10 in chick neural tube. (A) Immunostaining analyses with Chx10 and Myc antibodies for chick embryos electroporated (+ side) with Myc-Nkx6.1+LacZ, Myc-Nkx6.1+Rnf220+Zc4h2, Myc-Nkx6.1+Rnf220- Δ N+Zc4h2, Myc-Nkx6.1+Rnf220+Zc4h2-V63L or R198Q (thoracic level). (B) Quantification of Chx10⁺ neurons in the electroporated side (+) relative to those in the unelectroporated side (-) of chick neural tube. Values are means \pm s.d. *** $p < 0.001$, 'ns' indicates not significant.